Optics Communications 282 (2009) 1340–1344

Contents lists available at ScienceDirect

Optics Communications

journal homepage: www.elsevier.com/locate/optcom

Measurement of the quadratic Zeeman shift of ^{85}Rb hyperfine sublevels using stimulated Raman transitions

Run-Bing Li [a,b,c], Lin Zhou [a,b,c], Jin Wang [a,b,*], Ming-Sheng Zhan [a,b]

[a] State Key Laboratory of Magnetic Resonance and Atomic and Molecular Physics, Wuhan Institute of Physics and Mathematics, Chinese Academy of Sciences, P.O. Box 71010, Wuhan, Hubei 430071, China
[b] Center for Cold Atom Physics, Chinese Academy of Sciences, Wuhan 430071, China
[c] Graduate School, Chinese Academy of Sciences, Beijing 100080, China

ARTICLE INFO

Article history:
Received 6 September 2008
Received in revised form 28 November 2008
Accepted 11 December 2008

PACS:
32.80.Qk
03.75.Dg
37.25.+k

ABSTRACT

We demonstrate a technique for directly measuring the quadratic Zeeman shift using stimulated Raman transitions. The quadratic Zeeman shift has been measured yielding $\Delta\nu = 1296.8 \pm 3.3$ Hz/G^2 for magnetically insensitive sublevels ($5S_{1/2}, F = 2, m_F = 0 \rightarrow 5S_{1/2}, F = 3, m_F = 0$) of ^{85}Rb by compensating the magnetic field and cancelling the ac Stark shift. We also measured the cancellation ratio of the differential ac Stark shift due to the imbalanced Raman beams by using two pairs of Raman beams (σ^+, σ^+) and it is 1:3.67 when the one-photon detuning is 1.5 GHz in the experiment.

1. Introduction

Since the atom interferometer was demonstrated in 1991 [1], it has been applied to rotation measurement, such as inertial navigation and even the rotation rate of the earth [2,3]. Recently, an atom-interferometer gyroscope of high sensitivity and long-term stability was reported [4]. In order to improve the accuracy of the rotation rate measurement by using an atom-interferometer gyroscope, the potential systematic errors should be considered and controlled as well as possible. The quadratic Zeeman shift is considered as a factor that influences the accuracy of the rotation rate measurement in the atom-interferometer gyroscope.

The atom gyroscope generally uses two counter-propagating cold-atom clouds launched in strongly curved parabolic trajectories [3]. The two cold atom clouds should be overlapped completely in order to cancel common noise and gravity acceleration, and cold collisions occur between atoms along similar trajectories. For a dual atom-interferometer gyroscope, Rubidium is a suitable candidate because it has a smaller collision frequency shift than Cesium [5–8]. In our previous work [9,10], we have experimentally investigated the stimulated Raman transitions in the cold atom-interferometer. Both the accuracy and the fringe contrast of an atom-interferometer gyroscope can be improved by studying the magnetic field dependence of the coherent population transfer. A homogenous magnetic field must be applied along the Raman beams to keep the quantization axis consistent and resolve degenerate magnetic sublevels. This magnetic field will cause Zeeman shifts. The quadratic Zeeman shift induces a relative frequency shift of the two coherent states, which influences the accuracy of the rotation rate measurement. It is therefore important to measure accurately and understand the quadratic Zeeman shift of ^{85}Rb in the cold atom-interferometer. Similarly, the quadratic Zeeman shift is important in other applications such as microwave frequency standards [11–13], optical frequency standards [14,15] and coherent population trapping clock [16]. The quadratic Zeeman shift can be usually obtained from the Breit–Rabi formula after the magnetic field is measured by the linear Zeeman effect [17]. We study this from the field-insensitive clock transitions whose linear Zeeman shift is zero, thus the magnetic field is calibrated from other $u_F \neq 0$ states. We have also studied this quadratic Zeeman shift in the presence of the ac Stark shift of the Raman pulses.

In this paper, we analyze the hyperfine sublevels of the ground states in the magnetic field by using second-order perturbation theory, and demonstrate experimentally the coherent population transfer of the different Zeeman sublevels by stimulated Raman transitions. The quadratic Zeeman shift of the ground state of ^{85}Rb was measured by the two-photon resonance of the stimulated Raman transition after the ac Stark shift was cancelled and the

* Corresponding author. Address: State Key Laboratory of Magnetic Resonance and Atomic and Molecular Physics, Wuhan Institute of Physics and Mathematics, Chinese Academy of Sciences, P.O. Box 71010, Wuhan, Hubei 430071, China. Tel.: +86 27 8719 7375; fax: +86 27 8719 8576.
E-mail address: wangjin@wipm.ac.cn (J. Wang).

0030-4018/$ - see front matter © 2008 Elsevier B.V. All rights reserved.
doi:10.1016/j.optcom.2008.12.034

residual magnetic field was compensated. The value of the magnetic field is calibrated by the linear Zeeman shift. Our analysis shows that the quadratic Zeeman shift can be measured to Hz level for magnetically insensitive states ($5S_{1/2}, F = 2, m_F = 0 \rightarrow 5S_{1/2}, F = 3, m_F = 0$) in our experiment. We also measured the cancellation ratio of the differential ac Stark shift due to the imbalanced Raman beams by using two pairs of Raman beams. This study provides useful data for higher precision measurement of the quadratic Zeeman shift of ^{85}Rb, even for improving the accuracy of the rotation rate measurement of the atom-interferometer gyroscope.

2. Quadratic Zeeman shift

Including the hyperfine interaction, the ground state energy levels will split and shift in the magnetic field. The interaction Hamiltonian operator [18,19] within the subspace of hyperfine sublevels associated with the electronic levels is given by

$$H' = hA_S I \cdot J + g_J \mu_B J \cdot B + g_I \mu_B I \cdot B \tag{1}$$

where, h is the Plank constant, A_S is the hyperfine constant, I and J are the nuclear spin operators and orbital angular momentum, respectively, g_J and g_I are the electronic g-factor and nuclear g-factor, respectively, μ_B is Bohr magneton. Second-order perturbation theory is valid for low magnetic-field intensity, and the energies of the hyperfine Zeeman sublevels for the ground states can be derived as following

For $F = 2$

$$E\left(\frac{1}{2},2,0,B\right) = E\left(\frac{1}{2}\right) - \frac{7}{4}hA_S - \frac{(g_J - g_I)^2}{12hA_S}\mu_B^2 B^2 \tag{2}$$

$$E\left(\frac{1}{2},2,\pm 1,B\right) = E\left(\frac{1}{2}\right) - \frac{7}{4}hA_S \mp \frac{g_J - 7g_I}{6hA_S}\mu_B B - \frac{2(g_J - g_I)^2}{27hA_S}\mu_B^2 B^2 \tag{3}$$

$$E\left(\frac{1}{2},2,\pm 2,B\right) = E\left(\frac{1}{2}\right) - \frac{7}{4}hA_S \mp \frac{g_J - 7g_I}{3hA_S}\mu_B B - \frac{5(g_J - g_I)^2}{108hA_S}\mu_B^2 B^2 \tag{4}$$

For $F = 3$

$$E\left(\frac{1}{2},3,0,B\right) = E\left(\frac{1}{2}\right) + \frac{5}{4}hA_S + \frac{(g_J - g_I)^2}{12hA_S}\mu_B^2 B^2 \tag{5}$$

$$E\left(\frac{1}{2},3,\pm 1,B\right) = E\left(\frac{1}{2}\right) + \frac{5}{4}hA_S \pm \frac{g_J + 5g_I}{6hA_S}\mu_B B + \frac{2(g_J - g_I)^2}{27hA_S}\mu_B^2 B^2 \tag{6}$$

$$E\left(\frac{1}{2},3,\pm 2,B\right) = E\left(\frac{1}{2}\right) + \frac{5}{4}hA_S \pm \frac{g_J + 5g_I}{3hA_S}\mu_B B + \frac{5(g_J - g_I)^2}{108hA_S}\mu_B^2 B^2 \tag{7}$$

$$E\left(\frac{1}{2},3,\pm 3,B\right) = E\left(\frac{1}{2}\right) - \frac{7}{4}hA_S \pm \frac{g_J + 5g_I}{2hA_S}\mu_B B \tag{8}$$

Here, $E(J, F, m_F, B)$ denotes the energy of the hyperfine sublevels, including the effect of the hyperfine interaction and magnetic field splitting. From Eqs. (2) and (5), the quadratic Zeeman shift for the transition $5S_{1/2}, F = 2, m_F = 0 \rightarrow 5S_{1/2}, F = 3, m_F = 0$ is $\Delta\nu = (g_J - g_I)^2 \mu_B^2 B^2 / 6hA_S$, which is consistent with the Ref. [20] that is obtained from the Breit–Rabi formula when it is extended to second order in the field strength.

3. Experimental configuration

The experimental arrangement is shown in Fig. 1, which is similar to our previous work [9,10]. Briefly, the cold atoms are trapped in a nonmagnetic stainless steel chamber with 14 windows, where the trapping and repumping beams are provided by a tapered amplifier diode laser (TOPTICA TA100) and an external-cavity diode laser (TOPTICA DL100), respectively, whose frequencies are stabilized using saturated absorption spectroscopy [21]. After the polarization gradient cooling (PGC) process, the atoms are guided by a near-resonance laser pulse and fly transversely from the trapping region to the probe region at a velocity of 24 m/s [22]. Then, they are completely pumped to the ground state $5S_{1/2}, F = 2$ as the initial state by a perpendicular linearly polarized laser beam which is near resonance with the transition $5S_{1/2}, F = 3 \rightarrow 5P_{3/2}, F = 2$. Three crossed pairs of Helmholtz coils are used to provide the magnetic field in the Raman interaction area, where the current of the coils along the Raman beams (R_1,R_2) is controlled by the DC power supply (MPS-901) and measured by the digital multimeters (Flucke 8846A). The magnetic field intensity is calibrated by the first-order Zeeman shift, whose uncertainty is less than one part in one thousand. The combined Raman beams (R_1,R_2) and (R_1',R_2') are applied along the magnetic fields B and B_0, respectively, in the stimulated Raman interaction region. The Raman beams (R_1,R_2) are used to measure the frequency shift induced by the external fields such as the Raman beams (R_1',R_2') and the magnetic field B. The Raman beams (R_1,R_2) and (R_1',R_2') are supplied from the same Raman laser. This configuration has the benefit for the accurate measurement of the ac Stark shift because two pairs of Raman beams always have the same one-photon detuning. The detailed description of the Raman laser arrangement is similar to our previous work [10]. The atoms are transferred to the state $5S_{1/2}, F = 3$ from $5S_{1/2}, F = 2$ when they pass through a Raman π-pulse. After coherent population transfer via a simulated Raman transition, the population of the state is detected by a laser induced fluorescence (LIF) signal, and we use a photo multiplier tube (PMT) to collect the LIF.

4. Results and analysis

The hyperfine level $F = 2$ is split into five sublevels and $F = 3$ into seven sublevels, whose energies are expressed as in Eqs. (2)–(8) when there exists a magnetic field. After the magnetic field

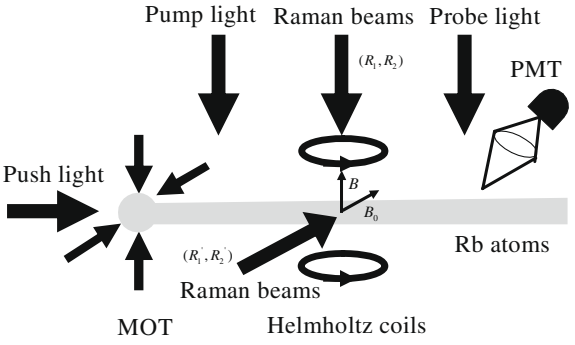

Fig. 1. Experimental scheme: cold ^{85}Rb atoms fly horizontally from the MOT to the probe region. Three crossed pairs of Helmholtz coils are applied to compensate the residual magnetic field in the stimulated Raman interaction area. The combined Raman beams (R_1,R_2) and (R_1',R_2') are parallel to the magnetic field B and B_0, respectively. The laser-induced fluorescence signal is detected by a PMT.

is compensated completely according to our previous work [9], all sublevels are degenerate. Coherent population transfer can occur for the transition of the combined hyperfine Zeeman sublevels $(-2,-2)$, $(-1,-1)$, $(0,0)$, $(1,1)$, $(2,2)$ when the Raman beams (R_1,R_2) with (σ^+,σ^+) propagate along the magnetic field B in the stimulated Raman interaction region as shown in Fig. 1 [9,23–25], where the Raman beams (R_1', R_2') and the magnetic field B_0 are not used. The maximum population transfer is achieved when two-photon resonance is satisfied with the transition selection rules shown in Fig. 2. A perfect symmetric Raman spectrum are achieved when the atoms are interacted with Raman beams (σ^+,σ^+). In Fig. 2, the transition probability can be explained using the oscillator strength of two-photon transition for the different hyperfine Zeeman sublevels $(-2,-2)$, $(-1,-1)$, $(0,0)$, $(1,1)$, $(2,2)$, respectively. The energy separation of the different sublevels is well explained by Eqs. (2)–(8) when the bias magnetic field $B = 220$ mG is applied. The magnetic field is calibrated by the linear Zeeman shift of the hyperfine Zeeman sublevels $(-2,-2)$ and $(2,2)$. For different magnetic field, we measured the resonance frequency for the transitions $(-2,-2)$ and $(2,2)$, as shown in Fig. 3. After a linear fit, the slope is the magnetic field intensity controlled by the current of the coils in the Raman interaction area. The scaled method is similar to that of the quadratic Zeeman shift measurement introduced in our paper. The scaled parameters come from earlier Refs. [20,26–28]. The scale factor of the magnetic field is 1576.9 ± 1.3 mG/A after the averaged measurements.

The differential ac Stark shift caused by the imbalanced Raman beams will induce a measurement noise in the determination of the quadratic Zeeman shift. The difference between the ac Stark shifts of two hyperfine sublevels, $\delta^{AC} = \Omega^{AC}_{F=3,m_F=0} - \Omega^{AC}_{F=2,m_F=0}$, can be cancelled by optimizing the ratio of two Raman beams [29]. We measure the frequency shift that is induced by one of the Raman beams separately. In the experiment, we use two pairs of Raman beams (R_1,R_2) and (R_1',R_2') along the magnetic field B and B_0, where B and B_0 are 250 mG and 100 mG, respectively. The Raman beams (R_1,R_2) are used to measure the ac Stark shift induced by the other Raman beams (R_1',R_2'). We carefully optimize the intensities of the Raman beams (R_1, R_2) along the magnetic field B to obtain a π-pulse. We scan the frequency difference of the Raman beams (R_1,R_2), and the resonant frequency of the hyperfine Zeeman sublevels (0,0) can be obtained by a Gaussian fit for the different Raman light intensities $(R_1'$, or $R_2')$. The detailed procedure is similar to test of quadratic Zeeman shift measurement in the paper. In the experiment, the Raman beams (R_1,R_2) and (R_1',R_2') are guided using single mode polarization maintained fiber. The intensity instability is below one part in one thousand for each of the Raman beams. The dots are the frequency shift that is induced by R_1', while the squares are the frequency shift that is induced by R_2' in Fig. 4, where they are fitted linearly. The slopes are 3.66 kHz/(mW/cm^2) and -0.99 kHz/(mW/cm^2) for R_1', and R_2', respectively. The frequency shifts, induced by the different Raman beams $(R_1'$, or $R_2')$, are referenced to the separation of hyperfine sublevels (3 035 732 436 Hz) [27]. The non null values are mainly caused by the quadratic Zeeman shift when the Raman beams (R_1', R_2') are not applied in Fig. 4. The ratio (1:3.67) of the two slopes determines the cancellation of the ac Stark shift when the one-photon detuning is 1.5 GHz in our experiment. Therefore, we can cancel the ac Stark shift by adjusting the ratio of two Raman beam intensities.

After the magnetic field compensation and the cancellation of the ac Stark shift, their influence is considerably decreased in the

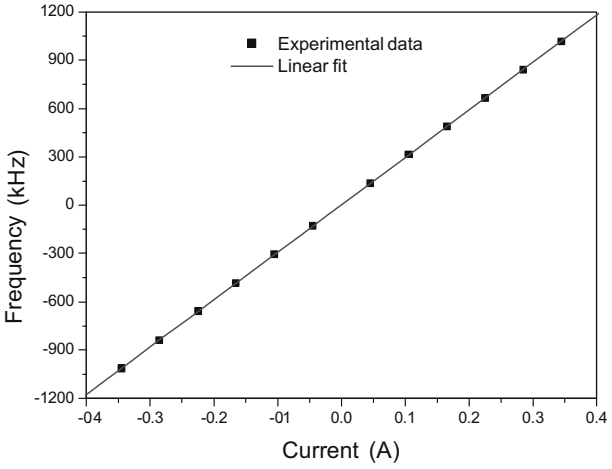

Fig. 3. The resonance frequency of the hyperfine Zeeman sublevels $(-2,-2)$ and $(2,2)$ depends on the current of the Helmholtz coils. It is measured by Raman beams (R_1,R_2) under $R_1' = 0$, $R_2' = 0$, $B_0 = 0$. The magnetic field can be scaled by the first-order Zeeman shift after the linear fit, whose uncertainty is below one per thousand.

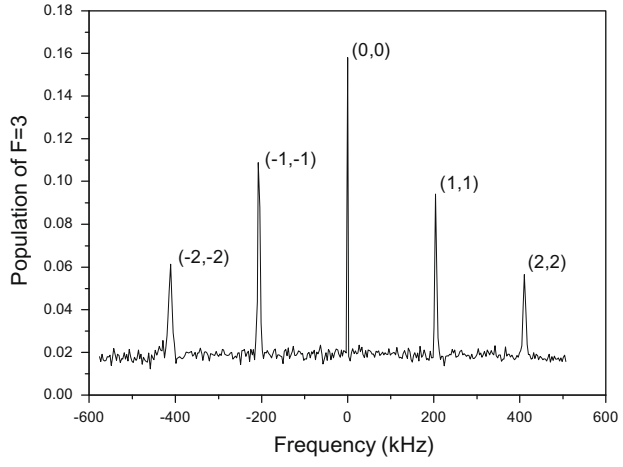

Fig. 2. Population transfer dependence on two-photon detuning. The peaks $(-2,-2)$, $(-1,-1)$, $(0,0)$, $(1,1)$, $(2,2)$ are the resonance transition of the hyperfine Zeeman sublevels when the Raman beams (R_1,R_2) are applied along the magnetic field $B = 220$ mG, where the Raman beams (R_1',R_2') and B_0 are not used.

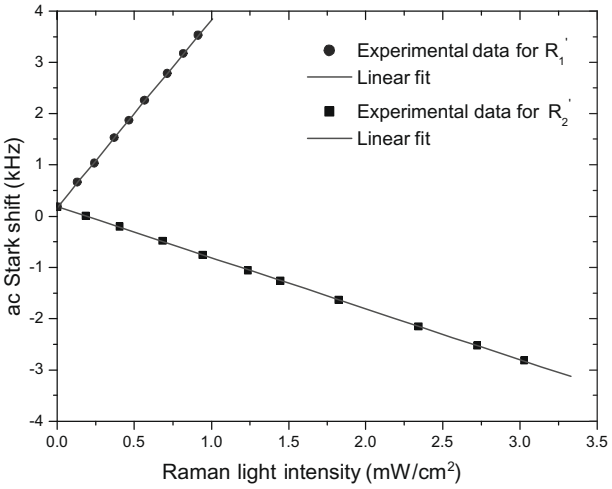

Fig. 4. The differential ac Stark shift caused by imbalanced Raman beams versus the Raman light intensity. The dots are the frequency shift induced by R_1' while the squares are the frequency shift induced by R_2', where they are fitted linearly and the slopes are 3.66 kHz/(mW/cm^2) and -0.99 kHz/(mW/cm^2), respectively. The ac Stark shift can be cancelled by adjusting the intensity ratio to 1:3.67 for the one-photon detuning $\Delta = 1.5$ GHz.

measurement of the quadratic Zeeman shift. The Raman beams are generated by an acousto-optical modulator (Brimrose, 1.5 GHz) driven by microwave generator (Agilent 8257 C) which is locked by a H-maser. The arrangement of the Raman laser is similar to our previous work [10]. We carefully optimize the intensities of the Raman beams (R_1, R_2) along the magnetic field B to obtain a π-pulse, where B_0, R_1' and R_2' are not used. The instability of the ratio of the Raman beams $(R_1 : R_2 = 1 : 3.67)$ is below 10^{-5} in the experiment. We scan the frequency difference of the Raman beams (R_1, R_2), and observe a typical stimulated Raman transition which shows the population versus frequency difference between the two Raman beams in Fig. 5 at a magnetic field $B = 600$ mG, where the frequency is referenced to the separation between the two ground states (3 035 732 436 Hz) [27]. In our experiment, the intensity profile of the Raman beams is a Gaussian distribution and the line width is mainly limited by the transition time because the spontaneous can be ignored in large one-photon detuning. In such case, the population dependence on the two-photon detuning is a Gaussian profile [30]. The central frequency is obtained from a Gaussian fit. We have made a series of such curves for different magnetic fields, and the dependence of the frequency shift on the magnetic field is shown in Fig. 6. The frequency shift depends

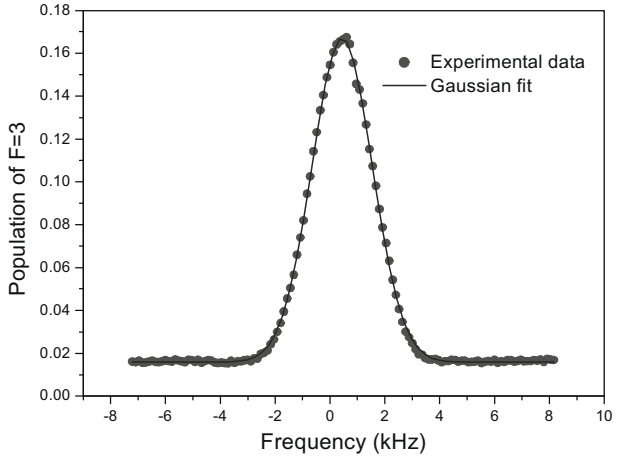

Fig. 5. Frequency dependence of transition amplitude for a square Raman π-pulse (R_1, R_2). The frequency is referenced to the hyperfine separation of the two ground states. The dots are the experimental data with $B = 600$ mG, $B_0 = 0$, $R_1' = 0$, $R_2' = 0$. while the solid line is the Gaussian fit.

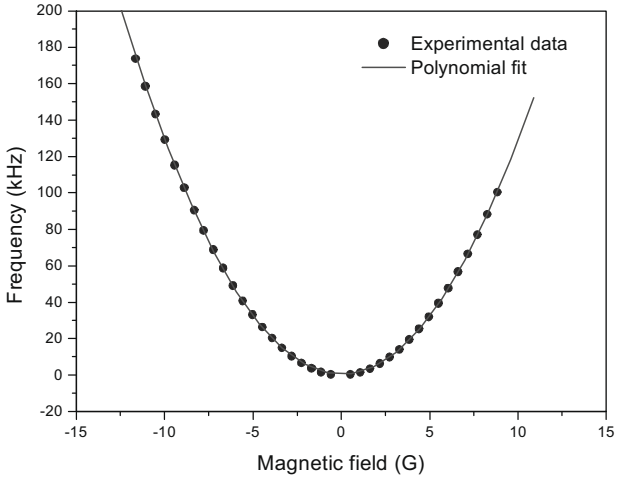

Fig. 6. Dependence of resonance frequency on the magnetic field intensity. The dots are the frequency shift in the different magnetic field that is obtained from Fig. 5, while the line is the experimental fit by a polynomial function.

Table 1
Experimental data for the determination of the quadratic Zeeman shift of hyperfine sublevels $(5S_{1/2}, F = 2, m_F = 0 \rightarrow 5S_{1/2}, F = 3, m_F = 0)$ of ^{85}Rb.

Run	Frequency shift (Hz/G^2)	Scaled error (Hz/G^2)	Fitted error (Hz/G^2)
1	1294.2	2.1	2.9
2	1294.1	2.1	2.9
3	1295.7	2.1	2.3
4	1296.1	2.1	2.2
5	1298.6	2.1	1.9
6	1298.7	2.1	1.9
7	1298.7	2.1	1.9
8	1298.6	2.1	1.9
Average	1296.8	2.1	2.5
Total	1296.8 ± 3.3 (Hz/G^2)		

on the magnetic field and it is fitted by a polynomial function (The maximum power is 2), while the quadratic dependence is for the quadratic Zeeman shift. We measured a series of values as shown in Table 1, and the average frequency shift induced by the quadratic Zeeman effect for the hyperfine Zeeman sublevels $(5S_{1/2}, F = 2, m_F = 0 \rightarrow 5S_{1/2}, F = 3, m_F = 0)$ is 1296.8 Hz/G^2. The measurement uncertainty comes mainly from the calibrated magnetic field and the fitted error. As shown in Table 1, the averaged uncertainty of the quadratic Zeeman shift is 2.1 Hz/G^2 and 2.5 Hz/G^2 for the scaled magnetic field and the fitted error, respectively. The final result for the quadratic Zeeman shift is 1296.8 ± 3.3 Hz/G^2 by using an independent error source model, which is in good agreement with the calculation result [20] within our measurement precision. The result shows that the second perturbation theory is sufficient when the magnetic field is less than 1 mT [19]. The ac Stark shifts induce a systematic shift of the ground-state hyperfine splitting. This does not influence the value of the quadratic Zeeman shift when a quadratic dependence term of the polynomial function is chosen as shown in Fig. 6. The fitted error, which is induced by the instability of the Raman beams, is decreased when the cancellation ratio of the Raman beams (1:3.67) is applied in the experiment.

In the atom-interferometer, the bias magnetic field is applied through the interference area. Although the atoms are always kept in magnetically insensitive states with $m_F = 0$, these states still show a quadratic Zeeman shift that induces a relative frequency shift of two ground states. This effect is big enough to require well controlled magnetic fields and extensive magnetic field shielding to achieve the millihertz frequency stability necessary for gravity measurements at the 1 μG level [23]. For the rotation rate measurement, the quadratic Zeeman shift should be known accurately when considering the accuracy necessary to determine the rotation rate of the earth. The sensitivity of the rotation signal to the various bias magnetic field was determined in detailly performed in the dual atomic interferometer gyroscope, and the bias magnetic field caused a phase shift $2 \times 10^{-6}\Omega_E$/mG for the rotation measurement in the system [24], which is mainly induced by the quadratic Zeeman shift. In our experiment, the precision of the quadratic Zeeman shift is mainly limited by the measurement time, and it can be measured even more accurately by decreasing the atomic flight velocity and increasing the Raman beam diameter, and by using the separated oscillation field method in a weak magnetic field [17]. However, our result provides helpful data for higher precision measurement of the quadratic Zeeman shift of ^{85}Rb, even for the accuracy of the rotation rate measurement of the atom-interferometer gyroscope.

5. Conclusion

In summary, we analyzed the energy of the hyperfine sublevels of two ground states of ^{85}Rb in the magnetic field. We demon-

strated experimentally the coherent population transfer of the hyperfine sublevels between two ground states by the stimulated Raman transition. The ac Stark shift was experimentally studied by measuring the ac Stark frequency shift dependence on the Raman beam intensity, and it was cancelled by adjusting the ratio of two Raman beam intensities. We measured the quadratic Zeeman shift of the ground states using the coherent population transfer by a stimulated Raman transition. The error analysis shows that the quadratic Zeeman shift was measured to Hz level for magnetically insensitive states $5S_{1/2}, F = 2, m_F = 0 \rightarrow 5S_{1/2}, F = 3, m_F = 0$ in the experiment. This result provides helpful data to improve the accuracy of the atom-interferometer gyroscope in future.

Acknowledgements

We acknowledge the financial support from the National Basic Research Program of China under Grant Nos. 2005CB724505, 2006CB921203, and from the National Natural Science Foundation of China under Grant No. 10774160. We thank Professor J. P. Connerade and Professor L. You for useful comment and discussion.

References

[1] M. Kasevich, S. Chu, Phys. Rev. Lett. 67 (1991) 181.
[2] T.L. Gustavson, A. Landragin, M. Kasevich, Class. Quantum Grav. 17 (2000) 2385.
[3] B. Canuel, F. Leduc, D. Holleville, A. Gauguet, J. Fils, A. Virdis, Phys. Rev. Lett. 97 (2006) 010402.
[4] D.S. Durfee, Y.K. Shaham, M.A. Kasevich, Phys. Rev. Lett. 97 (2006) 240801.
[5] F. Pereira Dos Santos, H. Marion, S. Bize, Y. Sortais, A. Clairon, Phys. Rev. Lett. 89 (2002) 233004.
[6] S.J.J.M.F. Kokkelmans, B.J. Verhaar, K. Gibble, D.J. Heinzen, Phys. Rev. A 56 (1997) R4389.
[7] K. Gibble, Phys. Rev. A 52 (1995) 3370.
[8] Y. Sortais, S. Bize, C. Nicolas, A. Clairon, Phys. Rev. Lett. 85 (2000) 3117.
[9] R.B. Li, P. Wang, H. Yan, J. Wang, M.S. Zhan, Phys. Rev. A 77 (2008) 033425.
[10] P. Wang, R.B. Li, H. Yan, J. Wang, M.S. Zhan, Chin. Phys. Lett. 24 (2007) 27.
[11] N.F. Ramsey, Molecular Beams, Oxford University Press, London, 1963. p. 127.
[12] J.E. Thomas, P.R. Hemmer, S. Ezekiel, Phys. Rev. Lett. 48 (1982) 867.
[13] P.R. Hemmer, G.P. Ontai, S. Ezekiel, J. Opt. Soc. Am. B 3 (1986) 219.
[14] M. Kajita, Ying, K. Matsubara, K. Hayasaka, M. Hosokawa, Phys. Rev. A 72 (2005).
[15] M.M. Boyd, T. Zelevinsky, A.D. Ludlow, S. Blatt, T.Z. Willette, S.M. Foreman, J. Ye, Phys. Rev. A 76 (2007) 022510.
[16] J. Vanier, Appl. Phys. B Laser Opt. 81 (2005) 421.
[17] S. Bize, Y. Sortais, M.S. Santos, C. Mandache, A. Clairon, C. Salomon, Europhys. Lett. 45 (1999) 558.
[18] I.I. Sobelman, Atomic Spectra and Radiative Transitions, Springer, New York, 1996. p. 61.
[19] W.M. Itano, J. Res. Natl. Inst. Stand. Technol. 105 (2000) 829.
[20] D.A. Steck, Rubidium 85 D Line Data, <http://steck.us/alkalidata>.
[21] J. Wang, X.J. Liu, J.M. Li, K.J. Jiang, M.S. Zhan, Chin. J. Quant. Electron. 17 (2000) 44.
[22] K.J. Jiang, K. Li, J. Wang, M.S. Zhan, Chin. Phys. Lett. 22 (2005) 324.
[23] A. Peters, Ph.D. Thesis, Stanford University, Palo Alto, CA, 1998.
[24] T.L. Gustavson, Ph.D. Thesis, Stanford University, Palo Alto, CA, 2000.
[25] T. Petelski, Ph.D. Thesis, University of Florence, Florence, 2005.
[26] P.L. Bender, E.C. Beaty, A.R. Chi, Phys. Rev. Lett. 1 (1958) 311.
[27] S. Penselin, T. Moran, V.W. Cohen, Phys. Rev. 127 (1962) 524.
[28] E. Arimondo, M. Inguscio, P. Violino, Rev. Mod. Phys. 49 (1977) 31.
[29] D.S. Weiss, B.C. Young, S. Chu, Appl. Phys. B 59 (1994) 217.
[30] W. Demtroder, Laser Spectroscopy Basic Concepts and Instrumentation, Springer, New York, 2003. p. 86.